ISAC-Oriented Beamforming Feedback Design and Optimization for WiFi Systems

Lei Huang, Yinghui He, *Member, IEEE*, Guanding Yu, *Senior Member, IEEE*, Jianfeng Wang, and Haiyan Luo

***Abstract*—With the widespread deployment of WiFi devices, utilizing beamforming feedback for sensing has become a popular trend in WiFi systems. However, the singular value decomposition (SVD)-based feedback method adopted in existing WiFi standards performs poorly in sensing performance since it only aims at maximizing the communication performance. To address this, we propose an integrated sensing and communication (ISAC)-oriented beamforming feedback protocol, which provides different sensing information based on the sensing indicator. Accordingly, we develop different ISAC-oriented CSI compression methods for different sensing applications requiring different feedback information. Taking the angle of departure (AoD) as an example, an optimization problem is formulated to maximize the data rate while preserving the complete AoD information. To resolve it, we propose an iterative algorithm to obtain the sub-optimal solution and a heuristic algorithm to reduce the computational complexity. We further extend the proposed compression method for the AoD information to the compression of the angle of arrival (AoA) and time of flight (ToF). Test results show that our proposal achieves both excellent communication and sensing performance and can be applied to various sensing applications, such as localization and action recognition.**

***Index Terms*—Integrated sensing and communication, beamforming feedback, WiFi system, channel state information.**

I. Introduction

Next-generation wireless systems are highly anticipated to bridge the physical and digital worlds, thereby providing intelligent services, such as smart transportation [1], [2], environmental monitoring [3], [4], and mobile healthcare [5], [6], rather than only pursuing high data rate [7]. To achieve this goal, wireless communications need to have the capability of sensing the physical world. To this end, both industry and academia have recently paid attention to one burgeoning technology, namely integrated communication and sensing (ISAC) [8]. Unlike traditional approaches where communication and sensing systems are separate [9], the ISAC technology aims to perform the sensing function on the same communication hardware and frequency bands, thereby offering the advantage of low overhead and high spectral efficiency [8], [10], [11].

Reusing pilot signals in existing communication systems for sensing is one of the most efficient solutions to realize ISAC [12]. Pilot signals, usually used for time synchronization and channel estimation, have low autocorrelation sidelobes, which is also the characteristic required by the sensing signals [13]. Thus, the measured channel state information (CSI) using pilot signals effectively captures information about the surrounding environment. However, the CSI is measured at the station (STA) using pilots transmitted by the access point (AP) and it needs to be further fed back to the AP for supporting the sensing applications (e.g., localization [14]–[16] and activity recognition [17], [18]) at the AP. Fully feeding back the complete CSI over different antennas and subcarriers to the AP would cause high overhead. To address this issue, most existing compression schemes [19], [20] focus solely on reducing the feedback volume from a communication perspective. However, such approaches may compromise the sensing information contained in the CSI, leading to a decrease in sensing precision. This issue is also highlighted in the ongoing WiFi standards, i.e., IEEE 802.11bf, aiming to explore the sensing capability in WiFi systems [21]. To this end, we aim to propose a novel ISAC-oriented feedback method for WiFi systems in this paper.

A. Related Works

Over the past few decades, WiFi sensing, enabled by extracting CSI from network interface cards (NICs), has attracted wide attention due to the widespread deployment of WiFi facilities, supporting activity recognition [17], [18], finger gesture recognition [22], breath detection [23], and localization [16], [24]. Specifically, Qian *et al.* proposed WiDance [17], a gesture-based interaction interface that extracts Doppler shifts and direction information from CSI for various activity recognition. Jiang *et al.* proposed EI [18], a deep-learning framework using convolutional neural networks (CNNs) to extract environment- and subject-independent CSI features for improved environmental independence. In addition to large-scale activity recognition, CSI is also used for small-scale activities like finger gesture identification and breath detection. For example, Wifinger [22] extracts CSI to detect subtle movements, and proposes an environmental noise removal mechanism to enhance the robustness of gesture recognition by mitigating signal dynamics. TensorBeat [23] leverages the CSI phase difference between the receiver and the transmitter, along with tensor decomposition techniques,

Manuscript received 27 October 2024; revised 1 February 2025; accepted 22 February 2025. (*Corresponding author: Yinghui He*)

L. Huang, Y. He, and G. Yu are with the College of Information Science and Electronic Engineering, Zhejiang University, Hangzhou 310027, China. e-mail: {22331141, 2014hyh, yuguanding}@zju.edu.cn.

J. Wang is with Lenovo Research, Lenovo Group Ltd., Beijing 100094, China. e-mail: wangjf20@lenovo.com.

H. Luo is with Lenovo (Shanghai) Information Technology Co., Ltd, Shanghai 201203, China. e-mail: luohy7@lenovo.com.

to achieve multi-user breathing rate estimation. Moreover, CSI can also be used for realizing localization, a crucial sensing application. For example, Kotaru *et al.* [16] proposed SpotFi which jointly estimates the angle of arrival (AoA) and time of flight (ToF) for improving resolution using CSI across different subcarriers and antennas. Unlike the previous work, Wang *et al.* [24] proposed LiFS, which utilizes the power fading model and the first Fresnel zone to realize model-based device-free localization.

However, extracting CSI requires specific NICs and hardware modifications [25], thus hindering the widespread adoption and further development of WiFi sensing. Therefore, attention has been turned to the clear-text channel feedback for beamforming in modern WiFi systems [26]. To reduce the overhead and ensure communication performance, existing WiFi standards, i.e., IEEE 802.11ac/ax, adopt the communication-oriented compression, i.e., singular value decomposition (SVD), to compress the CSI [19]. The compressed feedback can also be used for sensing [27]–[29]. Li *et al.* [27] used the Cramer-Rao bound (CRB) to quantify the sensing capability of the SVD-based feedback and proposed an efficient CRB-based feature selection algorithm. BeamSense [28] developed an innovative multi-path estimation algorithm that effectively maps compressed feedback to a multi-path channel using inherent fingerprints, and its sensing ability was verified with real-world tests. In addition, MUSE-Fi [29] achieved multi-person sensing applications such as respiration monitoring, gesture detection, and activity recognition by leveraging downlink beamforming feedback. Although existing works have proved that the SVD-based method can be used for sensing [27], [29], its performance is quite limited since CSI information is compressed for reducing the communication overhead, with a significant loss of sensing information [27]. To address this problem, Jiang *et al.* proposed a novel compression method [30], performing QR decomposition (QRD) on the conjugate transpose of the CSI matrix. This method ensures that the first column of the feedback matrix $\boldsymbol{Q}$ retains the complete angle of departure (AoD) information of the original CSI matrix. However, [30] only considers the sensing performance, which cannot be applied to the ISAC system that involves both sensing and communication performance.

B. Contribution

In this paper, we aim to develop an ISAC-oriented feedback method. Specifically, we face the following two issues. The first one is that different applications generally require different sensing information (e.g., AoD, AoA, and ToF). The existing solutions [22], [27], [30] fail to satisfy this requirement as they only feed back the same sensing information for different applications, which may lead to a poor sensing performance. The second one is how to effectively design the feedback jointly considering the communication and sensing. The existing SVD-based compression method focuses on maximizing communication performance and ignores part of sensing information, failing to support fine-grained WiFi sensing. On the other hand, the QRD-based method preserves a significant amount of original sensing information, while it does not consider the communication performance. The complete CSI feedback method, on the other hand, suffers from high overhead, especially with massive antennas.

To address the first issue, we first investigate existing sensing solutions and then propose a flexible feedback protocol, adapting to different sensing information requirements (e.g., AoD, AoA, and ToF) using a sensing indicator. To address the second issue, different from existing solutions, we adopt an optimization manner that balances communication and sensing performance, realizing high ISAC performance with minimal feedback overhead. Specifically, when the AoD information is required, we formulate an optimization problem aimed at maximizing the communication performance without compromising the AoD information. A sub-optimal iterative algorithm and a heuristic low-complexity algorithm are both developed with the consideration of the varying computation capability of STAs. This manner is also extended for other sensing information requirements. In summary, our main contributions are:

- To satisfy various requirements of different applications on the sensing information, we propose an ISAC-oriented flexible beamforming feedback protocol. It aims to provide necessary sensing information for different sensing applications and consists of corresponding ISAC-oriented compression methods that balance communication and sensing performance with minimal overhead.
- For the AoD information, we formulate an optimization problem to maximize the data rate while preserving the complete AoD information, and a sub-optimal iterative algorithm is developed to solve it. Moreover, a low-complexity algorithm is also developed with the computational complexity approaching that of the SVD. Our proposal is extended to other feedback scenarios, such as AoA and ToF.
- Test results demonstrate that compared with the QRD-based method, our proposal offers better communication performance while achieving more accurate distance estimation. In addition, compared with complete CSI, our proposal achieves comparable communication and sensing performance with lower feedback overhead and is adaptable to various sensing tasks.

C. Organization and Notations

The rest of this paper is organized as follows. Section II introduces the system model and provides our preliminary design. In Section III, we formulate the optimization problems for angle information. Sections IV and V introduce the compression methods for angle information, and the compression methods for ToF and complete CSI, respectively. Test results are presented in Section VI, and Section VII provides a summary of the whole paper.

In this paper, scalars are denoted by lower case, vectors are denoted by boldface lower case, and matrices are denoted by boldface upper case. $\boldsymbol{I}$ represents an identity matrix and $\mathbf{0}$ denotes an all-zero vector. $(\cdot)^T$ and $(\cdot)^H$ denotes transpose and Hermitian transpose, respectively. For a matrix $\boldsymbol{A}$, $\mathrm{tr}(\boldsymbol{A})$ is the

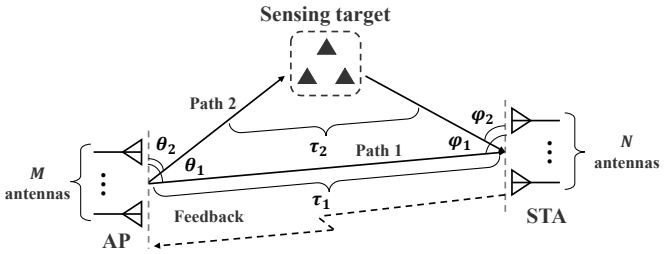

Fig. 1. A WiFi ISAC system where Path 1 represents the light-of-sight (LoS) path, Path 2 represents the non-LoS (NLoS) path, and the "feedback" describes the process of feeding the CSI after compression and quantization back to the AP.

trace of $\boldsymbol{A}$, $\boldsymbol{A}_{[n,m]}$ represents the element of $\boldsymbol{A}$ located in the n-th row and m-th column, and $\|\boldsymbol{A}\|$ denotes the Frobenius norm of $\boldsymbol{A}$. For a vector $\boldsymbol{a}$, $\|\boldsymbol{a}\|$ represents its Euclidean norm. $\mathbb{C}^{m\times n}$ denotes the space of $m \times n$ complex matrix.

II. System Model and Preliminary Design

In this section, we first introduce the system model and the channel model for the considered WiFi ISAC system. After that, we discuss the sensing information required by different sensing applications and present our preliminary design for CSI feedback.

A. System Model

As depicted in Figure (Fig.) 1, we consider a WiFi ISAC system consisting of an AP and a STA. Both the AP and STA adopt uniform linear array (ULA), and the numbers of antennas are N for the AP and M for the STA. The total bandwidth is divided into K subcarriers with the orthogonal frequency division multiplexing (OFDM) technique used in the system. The STA demands high-speed communication service, and the downlink beamforming technique is used at the AP to satisfy the requirement. Beginning with the 802.11ac standard, a channel sounding protocol has been adopted to support beamforming. It mainly contains three parts: pilot transmission, channel estimation, and feedback. After receiving the CSI feedback, the WiFi AP uses it to structure a beamforming matrix, denoted by $\boldsymbol{C}_k \in \mathbb{C}^{N\times M}$, for each subcarrier. Let $\boldsymbol{x}_k \in \mathbb{C}^{M\times 1}$ denote the transmit data at the WiFi AP for the k-th subcarrier. Then the received signal at the STA is

$$\boldsymbol{y}_k = \boldsymbol{H}_k\boldsymbol{C}_k\boldsymbol{x}_k + \boldsymbol{n}_k, \tag{1}$$

where $\boldsymbol{H}_k \in \mathbb{C}^{M\times N}$ is the wireless channel between the AP and STA and $\boldsymbol{n}_k \in \mathbb{C}^{M\times 1}$ is the additive white Gaussian noise (AWGN) following Gaussian distribution $\mathcal{CN}(0, \sigma^2\boldsymbol{I})$ with σ^2 being the noise power. The received signal is further processed with an equalizer, denoted by $\boldsymbol{B}_k \in \mathbb{C}^{M\times M}$, for recovering the transmit signal, as

$$\hat{\boldsymbol{x}}_k = \boldsymbol{B}_k\left(\boldsymbol{H}_k\boldsymbol{C}_k\boldsymbol{x}_k + \boldsymbol{n}_k\right). \tag{2}$$

Besides providing communication services, the AP also aims to deliver sensing information to support intelligent services, such as user localization and gesture recognition for ambient intelligence and smart environments [31], [32]. To this end, one possible solution is to transmit a sensing signal and collect the echo reflected by the sensing target via the full-duplex mode (like a monostatic radar [33]). However, such a mode requires expensive hardware and complex algorithms to realize self-interference cancellation, not practical for affordable consumer WiFi APs. As previously mentioned, the STA also feeds back the estimated CSI between the AP and itself to the AP, and the CSI also contains the sensing information as the pilot is reflected by the sensing target before arriving at the STA. Thus, in this paper, we aim to leverage the channel sounding protocol to realize WiFi ISAC, which is also urgently needed by the ongoing 802.11bf standard.

B. Channel Model and Sensing Basics

Following the ongoing 802.11bf standard, we adopt a ray-tracing-based channel model [34] in this paper. As shown in Fig. 1, the signal transmitted by the WiFi AP arrives at the STA through L effective propagation paths, and the AoD at the Wi-Fi AP, AoA at the STA, and ToF are θ_l, ϕ_l, and τ_l for the l-th path, respectively. Thus, the channel between the n-th antenna of the Wi-Fi AP and the m-th antenna of the STA for the k-th subcarrier can be expressed as

$$h_{m,n,k} = \sum_{l=1}^{L} \alpha_l e^{-j\pi((n-1)\sin(\theta_l)+(m-1)\sin(\phi_l)+2\tau_l f_k)}, \tag{3}$$

where $\alpha_l \in \mathbb{C}$ is the attenuation of the l-th path and f_k is the frequency of the k-th subcarrier. Note that we assume the antenna spacing is half a wavelength without loss of generality. Moreover, $h_{m,n,k}$ over different transmit and receive antennas makes up the CSI matrix as $\boldsymbol{H}_k = [h_{m,n,k}] \in \mathbb{C}^{M\times N}$ for each subcarrier.

From the channel model (3), one can clearly observe that AoD θ_l leads to the phase difference $\pi\sin(\theta_l)$ over different transmit antennas. Thus, when AoD information is required at the WiFi AP for supporting sensing applications, the CSI $h_{m,n,k}$ over different transmit antennas, i.e., one row of the CSI matrix $\boldsymbol{H}_k$, should be fed back to the AP via the channel sounding protocol. Note that scaling $h_{m,n,k}$ over different transmit antennas using the same factor does not influence the AoD information. Similarly, when the AoA/ToF information is required, the CSI $h_{m,n,k}$ over different receive antennas/subcarriers can be fed back to the AP.

C. The Overview of Our Design

The existing channel sounding protocol adopted in the 802.11ac/ax standard aims to realize maximum communication performance with minimal feedback. Thus, after estimating the channel at the STA, SVD [47] is adopted as $\boldsymbol{H}_k = \boldsymbol{U}_k\boldsymbol{\Sigma}_k(\boldsymbol{V}_k)^H$ and only the right unitary matrix $\boldsymbol{V}_k \in \mathbb{C}^{N\times M}$ is fed back to the AP after Givens rotation [48]. Then, $\boldsymbol{V}_k$ is directly used as the beamforming matrix at the AP as it is the optimal one for communication [49], [50]. This scheme only considers the communication performance while ignoring the sensing demand, and the sensing information contained in the CSI might be lost after applying the SVD. For example, the phase difference $\pi\sin(\theta_l)$ caused by AoD is destroyed since the SVD is not a simple scaling operation,

TABLE I
SUMMARY OF APPLICATIONS AND PROPOSED COMPRESSION METHODS FOR SENSING INFORMATION

Information	Sensing Applications	Compression methods
AoA/AoD	Localization [14], [35], [36], human pose recognition [37], human mesh construction [38].	Using two algorithms (the iterative algorithm and the low-complexity algorithm) in Section IV to obtain the matrix $\boldsymbol{C}_k$.
ToF	Localization [39], [40], multipath profiling [41].	Using SVD to obtain beamforming matrix $\boldsymbol{C}_k$. Using D-AMP or G-AMP in Section V-A to feed back the complete range information.
AoA/AoD + ToF	Localization [15], [42].	Using the compressed method for angle in Section IV to obtain the matrix $\boldsymbol{C}_k$. Using D-AMP or G-AMP in Section V-A to feed back the complete range information.
Complete CSI	Activity recognition [43], [44], finger gesture recognition [22], human breath detection [45], talking detection [46], localization [16], [24].	Using D-CSI or G-CSI in Section V-B to obtain the complete CSI.

and the accuracy of localization using $\boldsymbol{V}_k$ would be lower than that using the original CSI $\boldsymbol{H}_k$. To address this issue, Jiang *et al.* [30] applied QRD as $\boldsymbol{H}_k^H = \boldsymbol{Q}_k \boldsymbol{R}_k$, where $\boldsymbol{Q}_k \in \mathbb{C}^{N\times M}$ is a unity matrix and $\boldsymbol{R}_k \in \mathbb{C}^{M\times M}$ is an upper right-triangular matrix. Then, $\boldsymbol{Q}_k$ is fed back to the AP, which is later used as the beamforming matrix. Thanks to the characteristics of QRD, the first column of $\boldsymbol{Q}_k$ is the first column of $\boldsymbol{H}_k^H$ after normalization. Thus, the AoD information can be preserved and fed back to the AP without performance degradation. However, the QRD scheme only considers parts of sensing information, and the AoA information is still affected, which is not suitable for some sensing applications. Moreover, the communication performance has not been fully considered in the QRD scheme.

To address the aforementioned two issues, we propose a novel channel compression and feedback scheme for high-performance communication and sensing simultaneously. Different from the QRD scheme that mainly focuses on the AoD information, we consider the requirements of different sensing applications. We summarize the sensing information required for various tasks and corresponding compression methods in Table (Tab.) I. From the table, it is clear that some applications only require angle information (AoD or AoA). In such a case, we aim to use optimization to obtain the beamforming matrix that includes the complete angle information, as elaborated in Section IV. For applications that only require range information, i.e., ToF, we opt to feed back the beamforming matrix obtained through SVD, along with the CSI between the first transmit and receive antennas at different subcarriers, i.e., $\{h_{1,1,k}, \forall k\}$, compressed using D-AMP or G-AMP methods, which are detailed in Section V-A. Some applications require both angle and range information, in which case the beamforming matrix is obtained via optimization, and $\{h_{1,1,k}, \forall k\}$ are compressed using D-AMP or G-AMP methods. Additionally, some complex sensing applications demand the complete CSI matrix, for which we choose to feed back the entire CSI, compressed using D-CSI or G-CSI methods, as described in Section V-B.

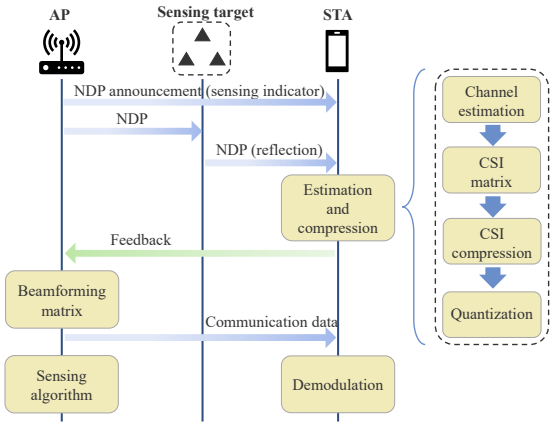

Fig. 2. The proposed ISAC-oriented channel sounding protocol.

We further develop a novel ISAC-oriented channel sounding protocol to overcome the limitation of existing works, as shown in Fig. 2. It is started by a null data packet (NDP) announcement transmitted by the AP. Different from the existing NDP announcement, it contains a sensing indicator for the required sensing information, listed in Table I.[1] A pilot, i.e., NDP, is transmitted after the NDP announcement, and the STA measures the CSI using the received NDP. The CSI matrix is compressed and quantified according to the received sensing indicator. The compressed CSI is further fed back to the AP. The AP performs sensing and communication functions based on the received information. For the multi-user scenario, our proposed methods can be easily extended following the existing multi-user beamforming feedback protocol [51].

In the next section, we will formulate the optimization problems for AoA/AoD information and solve them in Section IV. Moreover, the compression methods for ToF are detailed in Section V-A, and the compression methods for complete CSI are detailed in Section V-B.

[1]The indicator could be vacant for compatible with the existing protocol, i.e., requiring the compressed feedback using SVD for communication.

III. Problem Formulation for Angle Information

In this section, we focus on the angle information (AoD and AoA) and formulate mathematical problems for optimizing the beamforming matrix $\boldsymbol{C}_k$.

Firstly, we formulate the optimization problem for AoD information. According to the channel model mentioned in Section II-B, to keep the AoD information, we need to fully retain the first row of $\boldsymbol{H}_k$ in the beamforming matrix $\boldsymbol{C}_k$. Meanwhile, to ensure compatibility with existing WiFi systems, $\boldsymbol{C}_k$ should be unity, i.e., $\boldsymbol{C}_k^H\boldsymbol{C}_k = \boldsymbol{I}$, and the exisitng Givens rotation [48] can still be applied. Consequently, the first column of $\boldsymbol{C}_k$ should be equal to the normalized first row of $\boldsymbol{H}_k$ based on the data transmission expression in (1), as

$$\boldsymbol{C}_{k[:,1]} = \frac{1}{\|\boldsymbol{H}_{k[:,1]}^H\|}\boldsymbol{H}_{k[:,1]}^H, \tag{4}$$

where $\boldsymbol{A}_{[:,1]}^H$ is the first column of $\boldsymbol{A}^H$. We aim to improve the communication performance while maintaining the sensing performance. Meanwhile, we adopt the data rate as the metric for communication. Considering that WiFi standard is backward-compatible and most existing WiFi devices adopt zero-forcing (ZF) equalizer [52] for demodulation due to its low complexity and high performance, we also assume that STA uses the ZF equalizer, i.e., $\boldsymbol{B}_k = (\boldsymbol{H}_k\boldsymbol{C}_k)^{-1}$. Then, the signal after the equalizer can be expressed as

$$\begin{aligned}\hat{\boldsymbol{x}}_k &= \boldsymbol{x}_k + (\boldsymbol{H}_k\boldsymbol{C}_k)^{-1}\boldsymbol{n}_k \\ &= \boldsymbol{x}_k + \left(\boldsymbol{V}_k^H\boldsymbol{C}_k\right)^{-1}\boldsymbol{\Sigma}_k^{-1}\boldsymbol{U}_k^H\boldsymbol{n}_k.\end{aligned} \tag{5}$$

The signal-to-noise ratio (SNR) for each data stream at the k-th subcarrier can be expressed as

$$SNR_{k,m} = \frac{p_k}{\sigma^2\left((\boldsymbol{V}_k^H\boldsymbol{C}_k)^{-1}\boldsymbol{\Sigma}_k^{-2}(\boldsymbol{V}_k^H\boldsymbol{C}_k)^{-H}\right)_{[m,m]}}, \tag{6}$$

where p_k is the transmit power for each data stream. The overall data rate at the k-th subcarrier is

$$R_k = w\sum_{m=1}^{M}\log_2(1+SNR_{k,m}), \tag{7}$$

where w is the bandwidth occupied by each subcarrier.

Now, we can formulate the optimization problem for the beamforming matrix $\boldsymbol{C}_k$ as

$$\max_{\boldsymbol{C}_k} \quad w\sum_{m=1}^{M}\log_2(1+SNR_{k,m}), \tag{8a}$$

$$\text{s.t.} \quad \boldsymbol{C}_{k[:,1]} = \frac{1}{\|\boldsymbol{H}_{k[:,1]}^H\|}\boldsymbol{H}_{k[:,1]}^H, \tag{8b}$$

$$\boldsymbol{C}_k^H\boldsymbol{C}_k = \boldsymbol{I}. \tag{8c}$$

Since different subcarriers are independent in the OFDM system, we only focus on one single subcarrier, and other subcarriers can be dealt with in the same manner.

For AoA information, we only need to modify constraint (8b) in Problem (8) to $\boldsymbol{C}_{k[:,1:M]} = \boldsymbol{H}_{k[:,1]}$, ensuring that the feedback contains complete AoA information.

In Problem (8), the objective function (8a) is non-convex. The first constraint is linear and thus is convex. The second constraint is quadratic but is an equality constraint, which is apparently non-convex. As a result, solving Problem (8) is not easy due to the non-convex unitary constraint. In what follows, we will develop two algorithms to address the formulated optimization problem.

IV. Compression Methods for Angle Information

In this section, we first propose two algorithms (the iterative algorithm and the low-complexity algorithm) for Problem (8) and then extend the two algorithms for AoA information.

A. Iterative Algorithm for Problem (8)

First of all, we need to deal with the objective function since the relationship between the data rate and the beamforming matrix $\boldsymbol{C}_j$ are complex according to the SNR expression in (6). The total received signal power at the STA is $p_k\text{tr}\{\boldsymbol{C}_k^H\boldsymbol{H}_k^H\boldsymbol{H}_k\boldsymbol{C}_k\}$ according to equation (1) and we first opt to maximize the received power. Thus, we have the following lemma for $\boldsymbol{C}_k$.

Lemma 1. *For maximizing the received power, $\boldsymbol{C}_k$ should be*

$$\boldsymbol{C}_k = \boldsymbol{V}_k\boldsymbol{A}_k, \tag{9}$$

where $\boldsymbol{A}_k \in \mathbb{C}^{M\times M}$ is a unitary matrix.

Proof: Please refer to Appendix A. ∎

With Lemma 1, the SNR expression can be simplified as

$$SNR_{k,m} = \frac{p_k}{\sigma^2\boldsymbol{a}_{k,m}^H\boldsymbol{\Sigma}_k^{-2}\boldsymbol{a}_{k,m}}, \tag{10}$$

where $\boldsymbol{a}_{k,m} \in \mathbb{C}^{M\times 1}$ is the m-th column vector of $\boldsymbol{A}_k$. Meanwhile, constraint (8b) can be rewritten as

$$\boldsymbol{C}_{k[:,1]} = \boldsymbol{V}_k\boldsymbol{a}_{k,1}. \tag{11}$$

Thus, $\boldsymbol{a}_{k,1}$ can be directly derived, and we only need to focus on optimizing $\boldsymbol{a}_{k,m}$, $m = 2,\cdots,M$. To this end, we can easily derive the gradient of the data rate R_k on $\boldsymbol{a}_{k,m}$ ($m = 2,\cdots,M$), i.e., $\dfrac{\partial R_k}{\partial \boldsymbol{a}_{k,m}}$, and use it for updating the variable in each iteration.

However, due to unitary constraint (8c) in Problem (8), directly employing the gradient descent method would lead to an infeasible solution that violates the unitary constraint. To solve it, we aim to project the updated $\boldsymbol{A}_k^{(l)}$ in the l-th iteration into the set constructed by the unitary constraint with minimal modification on $\boldsymbol{A}_k^{(l)}$. Let $\boldsymbol{X}_k^{(l)} \in \mathbb{C}^{M\times M}$ denote the updated $\boldsymbol{A}_k^{(l)}$, and it can be obtained via solving the following problem:

$$\min_{\boldsymbol{X}_k^{(l)}} \quad \|\boldsymbol{A}_k^{(l)} - \boldsymbol{X}_k^{(l)}\|^2, \tag{12a}$$

$$\text{s.t.} \quad (\boldsymbol{X}_k^{(l)})^H\boldsymbol{X}_k^{(l)} = \boldsymbol{I}, \tag{12b}$$

$$\boldsymbol{X}_{k[:,1]}^{(l)} = \boldsymbol{a}_{k,1}. \tag{12c}$$

This problem aims to minimize the difference between the unitary matrix $\boldsymbol{X}_k^{(l)}$ and $\boldsymbol{A}_k^{(l)}$, whose optimal solution is given in the following theorem.

Theorem 1. *Given* $\hat{\boldsymbol{A}}_k^{(l)} = \boldsymbol{A}_{k[:,2:M]}^{(l)} - \boldsymbol{a}_{k,1}\boldsymbol{a}_{k,1}^H \boldsymbol{A}_{k[:,2:M]}^{(l)}$ *and its SVD being* $\hat{\boldsymbol{A}}_k^{(l)} = \boldsymbol{U}_k^{A,(l)} \boldsymbol{\Sigma}_k^{A,(l)} (\boldsymbol{V}_k^{A,(l)})^H$*, the optimal solution to Problem (12), denoted by* $\boldsymbol{X}_k^{(l),\star}$*, is*

$$\boldsymbol{X}_{k[:,2:M]}^{(l),\star} = \boldsymbol{U}_k^{A,(l)} (\boldsymbol{V}_k^{A,(l)})^H. \tag{13}$$

Proof: Please refer to Appendix B. ∎

Until now, we can summarize the whole iterative algorithm in Algorithm 1. First of all, we determine the first column of $\boldsymbol{A}_k$ using (11) with the computational complexity being $\mathcal{O}(NM)$. After that, we perform iteration for the remained columns of $\boldsymbol{A}_k$. Specifically, in each iteration, we first need to calculate gradient $\frac{\partial R_k}{\partial \boldsymbol{a}_{k,m}}$ for $m = 2, \cdots, M$, and the computational complexity is $\mathcal{O}(M^3)$. Then, we employ the Armijo rule to determine the step γ with the computational complexity being $\mathcal{O}((\log \frac{1}{\epsilon})M^2 + M^3)$ [53]. The Armijo rule applied is a commonly used line search criterion, primarily employed in optimization algorithms to ensure that each iteration results in a sufficient decrease in the objective function value. After that, we update $\boldsymbol{A}_k^{(l)}$ except for the first column and further project it to $\boldsymbol{X}_k^{(l)}$ using Theorem 1 for satisfying the unitary constraint, with the computational complexity being $\mathcal{O}(M^2)$ and $\mathcal{O}(M^3)$, respectively. Let I denote the number of iterations, and the overall computational complexity of the proposed iterative algorithm is

$$\mathcal{O}\left(I(M^3 + M^2 \log \frac{1}{\epsilon})\right). \tag{14}$$

Now, we analyze the convergence of Algorithm 1. Since we update the variable using the gradient descent method and the step is determined using the Armijo rule, the increase in each iteration, i.e., $R^{(l+1)} \geq R^{(l)}$, can be guaranteed. Meanwhile, the data rate has an upper bound since both the total transmit power and noise power are given. Consequently, Algorithm 1 converges to a sub-optimal solution to Problem (8).

Algorithm 1: Iterative Algorithm for Problem (8).

1. Initialize the maximal error tolerance ϵ, step γ, and the maximal number of iterations I. Set the iteration index l as 0;
2. Initialize $\boldsymbol{C}_k^{(0)}$ under the constraints (8b) and (8c);
3. Calculate the first column of $\boldsymbol{A}_k$, i.e., $\boldsymbol{a}_{k,1}$;
4. **repeat**
5. Calculate gradient $\frac{\partial R_k}{\partial \boldsymbol{a}_{k,m}}$;
6. Utilize the Armijo rule to determine the step γ;
7. Update $\boldsymbol{A}_k^{(l)}$ using gradient $\frac{\partial R_k}{\partial \boldsymbol{a}_{k,m}}$ and step γ;
8. Obtain $\boldsymbol{X}_k^{(l)}$ using updated $\boldsymbol{A}_k^{(l)}$ with Theorem 1;
9. $\boldsymbol{A}_k^{(l+1)} = \boldsymbol{X}_k^{(l)}$;
10. $l = l + 1$;
11. **until** *the norm of gradient is less than* ϵ *or* $l \geq I$.
12. **Output:** $\boldsymbol{C}_k = \boldsymbol{V}_k \boldsymbol{A}_k^{(l)}$.

B. Low-Complexity Algorithm for Problem (8)

For some STAs with low computation capacity, the iterative algorithm with high computational complexity would cause a large delay, and the cost mainly comes from the iteration. To address this issue, we aim to propose a low-complexity algorithm that does not need iteration in the following.

From the SNR expression in (10), the m-th data stream is only related to the m-th column vector $\boldsymbol{a}_{k,m}$ of $\boldsymbol{A}_k$, and $\{\boldsymbol{a}_{k,m}, \forall m\}$ are only coupled in the unitary constraint (8c). This drives us to successively optimize $\boldsymbol{a}_{k,m}$ for maximizing the corresponding m-th data stream's SNR, and the problem for optimizing $\boldsymbol{a}_{k,m}$ can be formulated as

$$\max_{\boldsymbol{a}_{k,m}} \quad SNR_{k,m} = \frac{p_k}{\sigma^2 \boldsymbol{a}_{k,m}^H \boldsymbol{\Sigma}_k^{-2} \boldsymbol{a}_{k,m}}, \tag{15a}$$

$$\text{s.t.} \quad ||\boldsymbol{a}_{k,m}|| = 1, \tag{15b}$$

$$\boldsymbol{a}_{k,m}^H \boldsymbol{a}_{k,m'} = 0, m' < m. \tag{15c}$$

The objective function of the above problem is further equivalent to minimize $\boldsymbol{a}_{k,m}^H \boldsymbol{\Sigma}_k^{-2} \boldsymbol{a}_{k,m}$. The difficulty of solving problem (15) still comes from unitary constraint (15c). To address it, we can derive the following feasible solution:

$$\boldsymbol{a}_{k,m} = \boldsymbol{Y}_{k,m} \hat{\boldsymbol{a}}_{k,m}, \ \forall m, \tag{16}$$

where $\boldsymbol{Y}_{k,m} \in \mathbb{C}^{M \times (M-m+1)}$ is a unitary matrix that lies in the null space of $\{\boldsymbol{a}_{k,m'}, m' < m\}$ and $\hat{\boldsymbol{a}}_{k,m} \in \mathbb{C}^{(M-m+1)\times 1}$ is treated as the optimization variable. Note that $\boldsymbol{Y}_{k,m}$ can be obtained using the Gram-Schmidt orthonormalization method [54]. With (16), it is readily to prove that $\boldsymbol{a}_{k,m'}^H \boldsymbol{a}_{k,m} = 0$ for $m' < m$ using recursion, and then we successively optimize $\hat{\boldsymbol{a}}_{k,m}$. The objective function can be rewritten as

$$\min_{\hat{\boldsymbol{a}}_{k,m}} \quad \hat{\boldsymbol{a}}_{k,m}^H \boldsymbol{Y}_{k,m}^H \boldsymbol{\Sigma}_k^{-2} \boldsymbol{Y}_{k,m} \hat{\boldsymbol{a}}_{k,m}. \tag{17}$$

Problem (17) can be easily solved using eigenvalue decomposition on $\boldsymbol{Y}_{k,m}^H \boldsymbol{\Sigma}_k^{-2} \boldsymbol{Y}_{k,m}$. Let $\boldsymbol{v}_{k,m} \in \mathbb{C}^{(M-m+1)\times 1}$ denote the eigenvector corresponding to the minimum eigenvalue of $\boldsymbol{Y}_{k,m}^H \boldsymbol{\Sigma}_k^{-2} \boldsymbol{Y}_{k,m}$. The optimal solution, denoted by $\hat{\boldsymbol{a}}_{k,m}^\star$, to Problem (17) is

$$\hat{\boldsymbol{a}}_{k,m}^\star = \boldsymbol{v}_{k,m}. \tag{18}$$

Note that the corresponding $\boldsymbol{a}_{k,m}^\star$ obtained using (16) satisfies the constraint (15b).

The overall low-complexity algorithm can be summarized in Algorithm 2. It contains a loop for sequentially optimizing $\boldsymbol{a}_{k,m}$. For $\boldsymbol{a}_{k,m}$, we first calculate $\boldsymbol{Y}_{k,m}$ with the computational complexity being $\mathcal{O}(M(M-m+1)^2)$, and the next step is to obtain $\boldsymbol{v}_{k,m}$. Since we only need to obtain the eigenvector of the minimum eigenvalue, it is not necessary to perform the whole eigenvalue decomposition. Instead, we can utilize the Lanczos algorithm [55], which can be used to efficiently find the external eigenvalues (maximum and minimum) and the corresponding eigenvector of a symmetric matrix, and its computational complexity for $\boldsymbol{v}_{k,m}$ is only $\mathcal{O}(t(M-m+1)^2)$, where $t \ll (M-m+1)$ denotes the number of iterations of Lanczos algorithm. After that, we use (16) to calculate $\boldsymbol{a}_{k,m}^\star$. Thus, the overall computational complexity of the Algorithm 2 is $\mathcal{O}(\frac{1}{6}M^2(M-1)(2M-1))$. This complexity can be further

Algorithm 2: Low-Complexity Algorithm for Problem (15).

Fix $\boldsymbol{a}_{k,1}$, and set column index m as 2;
repeat
  Calculate $\boldsymbol{Y}_{k,m}$;
  Use the Lanczos algorithm to obtain the eigenvector $\boldsymbol{v}_{k,m}$ corresponding to the smallest eigenvalue of $\boldsymbol{Y}_{k,m}^H \boldsymbol{\Sigma}_k^{-2} \boldsymbol{Y}_{k,m}$;
  $\hat{\boldsymbol{a}}_{k,m}^{\star} = \boldsymbol{v}_{k,m}$;
  $\boldsymbol{a}_{k,m}^{\star} = \boldsymbol{Y}_{k,m} \hat{\boldsymbol{a}}_{k,m}^{\star}$;
  $m = m + 1$;
until $m > M$.

reduced since the requirement on $\boldsymbol{Y}_{k,m}$ is that it contains all basis vectors in the null space of $\{\boldsymbol{a}_{k,m'}, m' < m\}$, and the requirement of being unitary is unnecessary. Thus, we can randomly generate a matrix $\boldsymbol{Y}_{k,1}$ before the loop. In the m-th iteration, we first select the last $(M - m + 1)$ columns of $\boldsymbol{Y}_{k,m-1}$ to construct $\boldsymbol{Y}_{k,m}$ and then apply orthogonalization to ensure that $\boldsymbol{a}_{k,m-1}^H \boldsymbol{y}_{k,m'} = 0$, $\forall m'$ with $\boldsymbol{y}_{k,m'}$ being the m'-th column vector of $\boldsymbol{Y}_{k,m}$. Finally, normalize each column of matrix $\boldsymbol{Y}_{k,m}$. Consequently, the computational complexity for $\boldsymbol{Y}_{k,m}$ in the m-th iteration is $\mathcal{O}((M - m + 1)M)$. Thus, the total computational complexity of Algorithm 2 is

$$\mathcal{O}\left(\frac{1}{6}(M-1)M((2t+3)M - t)\right), \tag{19}$$

approaching that of the SVD-based method.

C. Compression for AoA Information

In this section, we focus on AoA information. Similar to the compression for AoD information, we formulate an optimization problem and the difference is that the constraint on the first column of $\boldsymbol{C}_k$, i.e., $\boldsymbol{C}_{k[:,1]}$. Specifically, the first M elements of $\boldsymbol{C}_{k[:,1]}$ should be equal to the first column of $\boldsymbol{H}_{k[:,1]}$, i.e., $\boldsymbol{C}_{k[1:M,1]} = \boldsymbol{H}_{k[:,1]}$. To further apply the proposed Algorithms 1 and 2, $\boldsymbol{C}_k$ still needs to satisfy equation (11). However, it is worth worrying whether equation (11) can be ensured with $\boldsymbol{C}_{k[1:M,1]} = \boldsymbol{H}_{k[:,1]}$ or not since the size of $\boldsymbol{V}_k$ is only $N \times M$. To address this issue, we give the following lemma.

Lemma 2. *To satisfy equation* (11)*, we can structure remaining* $(N - M)$ *elements of* $\boldsymbol{C}_{k[:,1]}$ *with given first* M *elements of* $\boldsymbol{C}_{k[:,1]}$*, as*

$$\boldsymbol{C}_{k[M+1:N,1]} = \boldsymbol{V}_{k[M+1:N,:]} (\boldsymbol{V}_{k[1:M,:]})^{-1} \boldsymbol{C}_{k[1:M,1]}. \tag{20}$$

Proof: Please refer to Appendix C. ∎

With Lemma 2, we obtain $\boldsymbol{C}_{k[:,1]}$ and further normalize it to satisfy the unitary constraint. Until now, we can directly extend the proposed iterative algorithm and the low-complexity algorithm for AoA information.

V. Compression Methods for ToF and Complete CSI

In this section, we will introduce compression methods for ToF and complete CSI.

A. Compression for ToF Information

For some sensing applications, distance information is important. The estimation of distance d_l relies on the ToF τ_l, and the relationship between them is $d_l = \tau_l c$ where c is the speed of light. Recall that ToF leads to the phase difference $2\pi(\tau_l f_k)$ over different subcarriers in (3). Thus, CSI between the first transmit antenna and the first receive antenna at different subcarriers, i.e., $\{h_{1,1,k}, \forall k\}$, should be fed back to the AP for ToF. To maximize the communication performance, we adopt the SVD-based beamforming compression solution, and $\{h_{1,1,k}, \forall k\}$ are directly fed back to the AP. To this end, there are two different solutions. The first one, named D-AMP, is to directly quantify $\{h_{1,1,k}, \forall k\}$ individually and then feed them back to the AP. The second one, named G-AMP, is to use the Givens rotation [48] to compress the vector $[h_{1,1,1}, \cdots, h_{1,1,K}]$ into a series of angles and then feed the quantified angle back to the AP.

When the sensing application requires both angle and distance information, a compression method that jointly incorporates angle and distance information is required. Meanwhile, note that the compression method for angle does not conflict with that for distance, and thus we can directly combine the compression method for angle and that for distance. Taking AoD and ToF information as an example, we can feed $\boldsymbol{C}_k$ obtained using Algorithm 1 or 2 back to the AP for AoD. Meanwhile, we also need to feed back the compressed $\{h_{1,1,k}, \forall k\}$ using G-AMP or D-AMP method for ToF.

B. Compression for Complete CSI

As shown in Tab. I, there are also many sensing applications that require complete CSI. At this point, the compression methods for only angle and range information are no longer enough to support sensing applications. Thus, it is necessary to feed back the complete CSI matrix to the AP. Unlike the previous cases, each element of the feedback matrix is already determined in this case, and thus there is no optimization involved. The main issue we need to consider is how to compress the complete CSI matrix with minimal error. Similar to the method of ToF feedback in Section V-A, we propose two compression methods here.

- D-CSI method: Directly quantify the real and imaginary parts of each element in the CSI matrix and feed them back to the AP.
- G-CSI method: First, use SVD to obtain two unitary matrices $\boldsymbol{U}_k \in \mathbb{C}^{M \times M}$ and $\boldsymbol{V}_k \in \mathbb{C}^{N \times M}$, and a diagonal matrix $\boldsymbol{\Sigma}_k \in \mathbb{C}^{M \times M}$. Next, the Givens rotation is adopted to further compress the unitary matrices $\boldsymbol{U}_k$ and $\boldsymbol{V}_k$, converting them into a series of angles. Moreover, the appropriate number of quantization bits is selected to quantify these angles and diagonal elements of $\boldsymbol{\Sigma}_k$. Finally, all of them are fed back to the AP.

TABLE II
SIMULATION PARAMETERS.

Parameter	Value
Number of transmit antennas, N	4
Number of receive antennas, M	3
Bandwidth	20 MHz
Carrier frequency, f^{c}	5.18 GHz
Number of subcarriers, K	256
Distance of path 1, d_1	10 m
Distance of path 2, d_2	15 m
Angles of path 1, (θ_1, φ_1)	$(0°, 0°)$
Angles of path 2, (θ_2, φ_2)	$(40°, -30°)$
SNR	20 dB
MCS index	5

In practice, we can choose one of the quantization methods according to the requirement on the sensing performance. Taking the action recognition task as an example, we can determine the relationship between the number of quantization bits and the sensing accuracy for both methods during the training phase. During the application phase, the AP can select the number of quantization bits and the method according to the required sensing accuracy.

VI. TEST RESULTS

In this section, we use simulations to verify the communication and sensing performance of the proposed methods. After that, a realistic experiment is conducted to further verify the sensing performance of the proposed methods.

A. Simulation Parameters

The simulation settings are outlined below unless stated otherwise. We adopt WiFi 6 standard with the carrier frequency being 5.18 GHz, i.e., $f^{\mathrm{c}} = 5.18$ GHz. The AP and STA work under a bandwidth of 20 MHz, and the number of subcarriers is 256, i.e., $K = 256$. The numbers of antennas at the AP and STA are 4 and 3, respectively, i.e., $N = 4$ and $M = 3$. For the wireless channel between the AP and STA, we adopt the ray-tracing-based channel model mentioned in Section II-B, consisting of multiple paths. Among these paths, the attenuation of two paths is observably weaker than others. Path 1 corresponds to the LoS path with a distance of 10 meters, i.e., $d_1 = 10$ m, and both AoD and AoA are $0°$, i.e., $(\theta_1, \phi_1) = (0°, 0°)$. It can be used for active localization. Path 2 corresponds to the NLoS path with a distance of 15 meters, i.e., $d_2 = 15$ m. The AoD and AoA are $40°$ and $-30°$, respectively, i.e., $(\theta_2, \phi_2) = (40°, -30°)$. It can be used for passive localization. The SNR is set as 20 dB and the modulation coding scheme (MCS) index is set as 5. The major simulation parameters are summarized in Tab. II.

B. Communication Performance

We first focus on the communication performance and compare the proposed methods with the existing SVD-based method and QRD-based method [30]. Fig. 3 shows the communication performance under different SNRs between the AP and STA with the metrics being throughput and packet error rate (PER). First of all, the communication performance of all methods increases with the SNR since the increase of the transmit power is beneficial for correct demodulation. Then, one can clearly observe that the SVD-based method offers the best communication performance i.e., the highest throughput and the lowest PER, because the beamforming feedback generated by the SVD is solely designed for communication. When the AP requires AoD information, the proposed methods (both the iterative and low-complexity algorithms) outperform the QRD-based method in terms of communication performance, verifying the superiority of our proposals. Although the first column of the feedback matrix in the proposed methods is the same as that in the QRD-based method, the remaining columns are optimized for maximizing the communication performance. As a result, the proposed methods could realize better communication performance than the QRD-based method. Additionally, in the proposed methods, the performance of the low-complexity algorithm is slightly worse than the iterative algorithm, which indicates that the low-complexity algorithm trades a slight performance degradation for a significant reduction in complexity. Moreover, when the AP requires AoA information, although the performance of our proposals fluctuates, we still can observe that the proposed methods outperform the QRD-based method, further confirming the effectiveness and stability of the proposals. Besides, it is noted that our proposals are more suitable for devices with low communication demands, such as smart speakers. They only need to maintain basic communication functionality and have high demands for sensing the surrounding environment. If the device has higher communication requirements, the SVD method can still be chosen.

We show the running time of the proposed methods and the two baselines in Tab. III. All methods are implemented on a

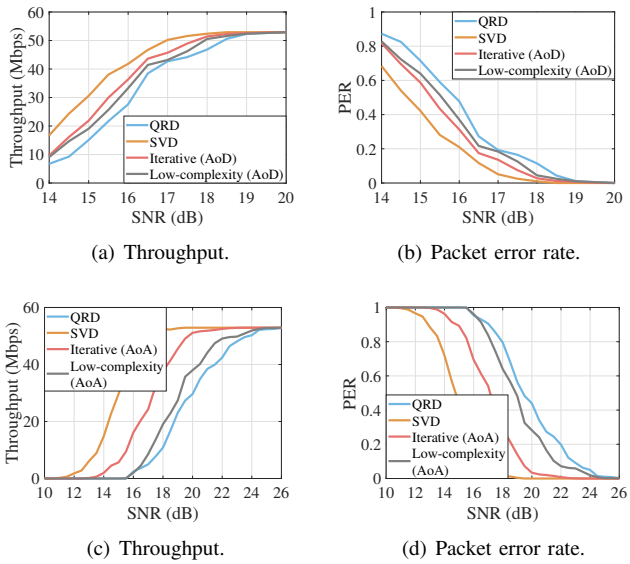

(a) Throughput. (b) Packet error rate.

(c) Throughput. (d) Packet error rate.

Fig. 3. Communication performance under different SNRs, where (a) and (b) show the performance of the proposal when AoD is required, and (c) and (d) show the performance of the proposal when AoA is required.

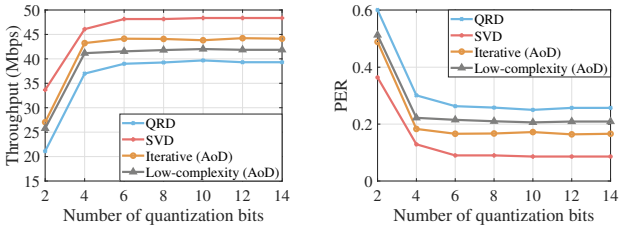

(a) Throughput. (b) Packet error rate.

Fig. 4. Communication performance under different numbers of quantization bits.

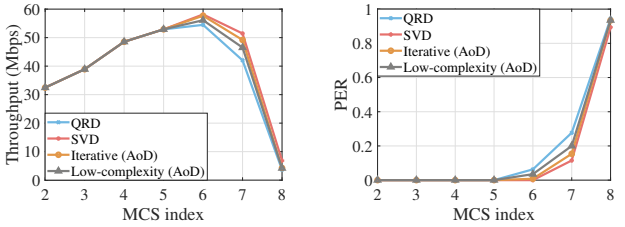

(a) Throughput. (b) Packet error rate.

Fig. 5. Communication performance under different MCS indices.

TABLE III
RUNNING TIME COMPARISON.

Compression methods	Running time (s)
SVD	3.71×10^{-3}
QRD	2.02×10^{-3}
Iterative algorithm (AoD)	8.08×10^{-1}
Low-complexity algorithm (AoD)	5.32×10^{-3}

personal computer equipped with an Intel i5-8265U CPU and 8 GB RAM. It can be observed that the running time of the low-complexity algorithm is significantly lower than that of the iterative algorithm and is close to that of the SVD method and QRD method. Thus, the low-complexity algorithm can be used in the real-time communication scenario.

Fig. 4 shows the communication performance under different numbers of quantization bits for the proposed methods and the two baselines. It can be observed that the communication performance for all methods improves as the number of quantization bits increases. This is because the increase in the number of quantization bits enhances precision, allowing the AP to recover more accurate feedback matrices. When the number of quantization bits is higher than 6, the improvement in the communication performance for each method becomes quite limited. Therefore, in practice, setting the number of quantization bits to 6 in WiFi systems can achieve high communication performance while reducing feedback overhead, which is a suitable choice. Besides, we can observe that the proposed methods outperform the QRD-based method under the same number of quantization bits. This result indicates that the proposed methods can achieve the same communication performance with less number of quantization bits, reducing the overhead.

Fig. 5 shows the communication performance under different MCS indices for four schemes. It can be found that the performance of both proposed iterative and low-complexity

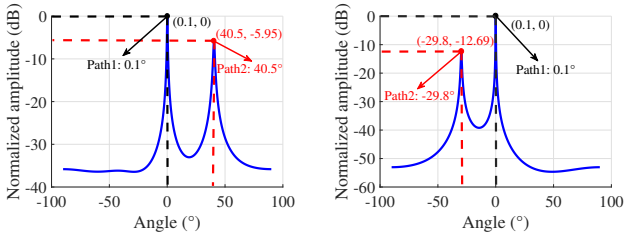

(a) AoD. (b) AoA.

Fig. 6. Angle estimation results for the proposed method.

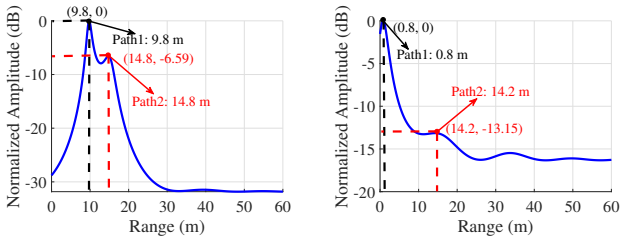

(a) The proposed method. (b) QRD-based method.

Fig. 7. Performance comparison on distance estimation.

algorithms is higher than that of the QRD-based method, further confirming the effectiveness of the proposal. Moreover, the PER increases with the MCS index since the received signal is easier to be misjudged with higher MCS under the same SNR. Consequently, when the MCS index is low, the increase in the MCS index leads to an increase in the throughput since a higher MCS index allows more data to be transmitted, with only a slight increase in the PER. However, when the MCS index becomes high, the increase in the MCS index leads to a decrease in the throughput since the increase in the PER is remarkable, and most of the data cannot be correctly decoded.

C. Sensing Performance

To measure the sensing performance of the proposed methods, we consider the sensing application of localization in this part. The feedback matrix at the AP is further used for determining the AoD/AoA and ToF using the multiple signal classification (MUSIC) algorithm [56]. First of all, we focus on the individual parameter estimation. Fig. 6 shows the estimation results of AoD and AoA using the proposed method. From it, one can clearly observe that both of them can be accurately estimated since the CSI at the first transmit/receive antenna is fed back to the AP without any modification. For the estimation of ToF, we compare our proposed method with the QRD-based method, and the corresponding result is plotted in Fig. 7. The main difference between the two methods is that our method feeds $\{h_{1,1,k}, \forall k\}$ back to the AP while the QRD-based method does not. We observe that the proposed method is more accurate for distance estimation than the QRD-based method, and the QRD-based method shows a significant peak shift. This result is reasonable since the QRD-based method loses part of the distance information. Moreover, we also plot the estimation results in Fig. 8 when the distance difference between the two paths becomes more obvious, i.e., $d_1 = 15\,\text{m}$ and $d_2 = 40\,\text{m}$. It can be seen that the performance of the

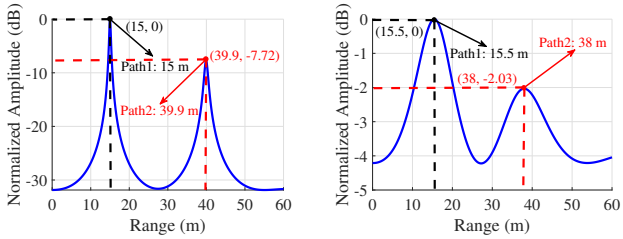

(a) The proposed method. (b) QRD-based method.

Fig. 8. Performance comparison on distance estimation when the two paths differ significantly.

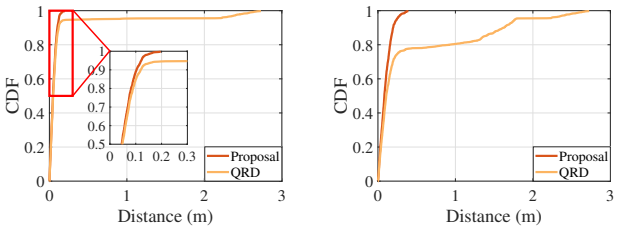

(a) LoS. (b) NLoS.

Fig. 9. Comparison of CDFs for range deviation.

QRD-based method is still lower than that of our proposed method. This result further verifies the effectiveness of the proposed method.

To further demonstrate the superiority of the proposed method in distance estimation, we generate 1,000 random channels and plot the cumulative distribution function (CDF) of the estimation error for both the LoS path and NLoS path in Fig. 9. From the figure, one can clearly observe that the estimation error of the proposed method is mainly less than 0.2 meter for the LoS path. In contrast, the estimation error of the QRD-based method would be more than one meter with the probability of 4.6%. Moreover, for the NLoS path, the superiority of the proposed method in the distance estimation is more pronounced, because the signal in the NLoS path is weaker than that in the LoS path and thus $\{h_{1,1,k}, \forall k\}$ has a greater impact on the estimation. All the above results verify the effectiveness of our proposed method.

Based on the above discussion, we conclude that the feedback of $\{h_{1,1,k}, \forall k\}$ is necessary for distance estimation. Now, we aim to explore the performance of the proposed two quantization methods in Section V-A for $\{h_{1,1,k}, \forall k\}$. Tab. IV presents the total feedback amount and sensing performance (measured by the median distance deviation) with different numbers of quantization bits for both feedback methods. For example, in the first line, the D-AMP method uses 5 bit to quantify the real/imaginary part of $h_{1,1,k}$, and the G-AMP method uses 4 bit and 6 bit to quantify the two types of angles after applying Givens rotation [48], respectively. We can observe that the total feedback amount for D-AMP and G-AMP is similar, with G-AMP being slightly smaller than D-AMP. When the number of quantization bits is small, G-AMP's distance deviation is less than that of D-AMP for both the LoS and NLoS paths. As the number of quantization bits increases, the distance deviation for both methods gradually decreases, and the performance difference diminishes. Therefore, with a small number of quantization bits, we can adopt

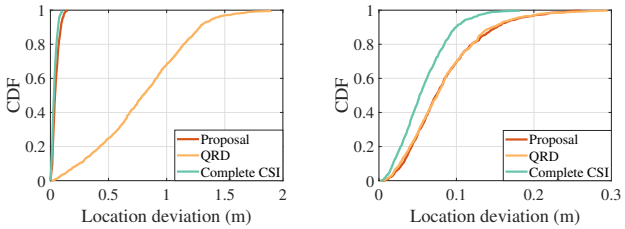

(a) LoS. (b) NLoS.

Fig. 10. CDFs of localization estimation error.

TABLE IV
COMPARISON OF THE PROPOSED TWO METHODS FOR TOF.

Schemes	Feedback (bits)	Median deviation (m) LOS	NLOS
D-AMP: 5 bit	2,560	1.61×10^{-2}	4.68×10^{-2}
G-AMP: 4 bit and 6 bit	2,550	8.30×10^{-3}	2.87×10^{-2}
D-AMP: 6 bit	3,072	2.40×10^{-3}	2.08×10^{-2}
G-AMP: 5 bit and 7 bit	3,060	7.61×10^{-4}	1.70×10^{-3}
D-AMP: 7 bit	3,584	9.74×10^{-4}	3.40×10^{-3}
G-AMP: 6 bit and 8 bit	3,570	7.61×10^{-4}	1.70×10^{-3}
D-AMP: 8 bit	4,096	7.68×10^{-4}	9.54×10^{-4}
G-AMP: 7 bit and 9 bit	4,080	7.60×10^{-4}	7.93×10^{-4}
D-AMP: 9 bit	4,608	6.75×10^{-4}	6.89×10^{-4}
G-AMP: 8 bit and 10 bit	4,590	6.75×10^{-4}	6.89×10^{-4}

G-AMP to compress $\{h_{1,1,k}, \forall k\}$ for achieving higher sensing performance.

After studying the estimation performance for each parameter individually, we now show the localization performance. Here, we aim to estimate the location of the STA and a target using the LoS path and the NLoS path, respectively. To show the average performance, we generate 1,000 random channels using the channel model in (3). Specifically, the AP's location is fixed, but the locations of the STA and the target are varying, leading to the varying LoS path and NLoS path. To estimate the location of STA, we adopt the compression method that jointly considers AoD and ToF introduced in Section V-A and then apply the MUSIC algorithm to obtain the AoD and ToF of the LoS path. We compare the proposed method with the QRD-based method and the scheme using complete CSI without compression, and the results are shown in Fig. 10(a). It can be seen that the performance of the proposed method approaches that of using complete CSI, demonstrating its high sensing capability. Moreover, the QRD-based method shows a much lower performance than the other two methods since it only feeds part of the distance information back to the AP, causing inaccurate estimation of distance.

Next, we aim to estimate the location of the target. To this end, we need both AoA and AoD information of the NLoS path, and it can be realized via double feedback. The first one uses the method for AoD feedback introduced in Section IV and the second one uses the method for AoA feedback introduced in Section IV-C. Meanwhile, we adopt the aforementioned two baselines. Note that the QRD-based method also needs double feedback. The estimation results for three different methods are shown in Fig. 10(b). It can be observed that the performance of the QRD-based method is similar to the proposed method, as the target's location

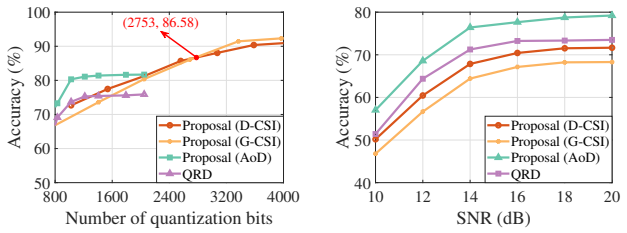

(a) Number of quantization bits. (b) SNR.

Fig. 11. The effect of the number of quantization bits and SNR on the recognition accuracy.

estimation uses angle information (AoD and AoA) and the accuracy of angle estimation is similar between the QRD-based method and the proposed method. The localization accuracy of using complete CSI is higher than the proposed method, because it contains complete sensing information. However, using complete CSI for localization requires high overhead and thus may not be adopted in practical systems.

D. Experiments for Sensing

In this section, we focus on the sensing application of action recognition. To this end, we utilize a sensing dataset collected using two USRP B210 [57]. The dataset includes eight different behaviors, i.e., standing still, kicking, raising a hand, waving, bending down, walking, sitting down, and standing up, with eight volunteers. The total number of CSI time series in the dataset is 3,200 with 2,560 CSI time series used for training and 640 time series used for testing. We apply the proposed methods and the QRD-based method in each CSI matrix contained in the time series for simulating the compression. Moreover, the ResNet is adopted for realizing action recognition. Note that the recognition accuracy is influenced by both the complexity of the dataset and the network used for recognition, and we focus on presenting the performance improvement of our proposed method in comparison to the baseline.

Here, we consider four methods: the D-CSI method, the G-CSI method, the proposed method for AoD in Section IV, and the QRD-based method. The first two methods proposed in Section V-B aim to feed back the complete CSI to the AP, the third one mainly feeds back the AoD-related sensing information, and the last one is used as a baseline. The recognition accuracy of the four methods under different numbers of quantization bits is depicted in Fig. 11(a). Notably, when the total number of quantization bits is small, using complete CSI (i.e., the D-CSI and G-CSI methods) for action recognition results in lower accuracy compared to the compressed methods for AoD information (i.e., the proposed and QRD-based methods). The main reason is that the CSI received at the AP is severely distorted with a small number of quantization bits, resulting in the loss of sensing information and low recognition accuracy. The advantages of feeding back complete CSI appear under a large number of quantization bits. Besides, by comparing the D-CSI with G-CSI methods, it can be seen that the D-CSI method outperforms the G-CSI method when the total number of quantization bits is less than 2,753. This value can be regarded as the threshold for choosing the appropriate method. Additionally, the performance of the proposed method and QRD-based methods for AoD almost keeps a constant when the number of quantization bits is higher than 1,500, and their performance upper limit is lower than those of the D-CSI and G-CSI methods since the former two methods abandon part of sensing information. Given the number of quantization bits being 1,024, we plot the recognition accuracy under different SNRs in Fig. 11(b). It can be seen that the accuracy of all four methods increases with the SNR since the CSI can recover the sensing target's information more accurately with higher SNR, thus improving the accuracy. Moreover, the performance of the proposed compression method for AoD is higher than that of the QRD-based method, further verifying the superiority.

VII. Conclusion

In this paper, we have proposed an ISAC-oriented beamforming feedback compression mechanism that simultaneously considers both sensing and communication performance. Depending on the requirements of different sensing applications, we first proposed an ISAC-oriented channel sounding protocol with a sensing indicator for different required information and further developed the corresponding compression methods. To be specific, for the AoD information, we formulated a throughput maximization problem under the constraint of sensing information. Both an iterative algorithm and a low-complexity algorithm were proposed to solve it for realizing compression. Furthermore, the compression method was extended for obtaining other sensing information. Extensive test results verified the excellent performance of the proposed method in both communication and sensing by comparing it with several existing methods.

Appendix A
Proof of Lemma 1

$\boldsymbol{C}_k$ can be divided into two parts. The first part is in the space constructed by $\boldsymbol{V}_k$ with the coefficient matrix $\boldsymbol{A}_k \in \mathbb{C}^{M\times M}$, and the second part is the null space of $\boldsymbol{V}_k$, denoted by $\bar{\boldsymbol{V}}_k \in \mathbb{C}^{N\times(N-M)}$, with the coefficient matrix $\bar{\boldsymbol{A}}_k \in \mathbb{C}^{(N-M)\times M}$. Thus, $\boldsymbol{C}_k$ can be expressed as $\boldsymbol{C}_k = \boldsymbol{V}_k\boldsymbol{A}_k + \bar{\boldsymbol{V}}_k\bar{\boldsymbol{A}}_k$. Since $\boldsymbol{C}_k^H\boldsymbol{C}_k = \boldsymbol{I}$, we have

$$\boldsymbol{A}_k^H\boldsymbol{A}_k + \bar{\boldsymbol{A}}_k^H\bar{\boldsymbol{A}}_k = \boldsymbol{I}. \tag{21}$$

Meanwhile, $\mathrm{tr}\{\boldsymbol{C}_k^H\boldsymbol{H}_k^H\boldsymbol{H}_k\boldsymbol{C}_k\}$ can be rewritten as

$$\begin{aligned}&\mathrm{tr}\{\boldsymbol{C}_k^H\boldsymbol{V}_k\boldsymbol{\Sigma}_k^2\boldsymbol{V}_k^H\boldsymbol{C}_k\boldsymbol{P}_k\}\\ =&\mathrm{tr}\{\boldsymbol{\Sigma}_k^2\boldsymbol{A}_k\boldsymbol{A}_k^H\} \overset{(a)}{\leq} \sum_{m=1}^{M}\sigma_{k,m}^2|\lambda_{k,m}|^2,\end{aligned} \tag{22}$$

where $\sigma_{k,m}$ is the m-th diagonal element of $\boldsymbol{\Sigma}_k$, $\lambda_{k,m}$ is the m-th eigenvalue of $\boldsymbol{A}_k$, and (a) is derived based on Von Neumann's inequality [58]. According to (21), the norm of each eigenvalue for $\boldsymbol{A}_k$ is no more than 1. Therefore, the total received power is no more than $\sum_{m=1}^{M}\sigma_{k,m}^2$. We note that the upper limit can be achieved when $\boldsymbol{A}_k\boldsymbol{A}_k^H = \boldsymbol{I}$ and $\bar{\boldsymbol{A}}_k$ should be zero, which ends the proof.

APPENDIX B
PROOF OF THEOREM 1

First of all, $\|\boldsymbol{A}_k^{(l)} - \boldsymbol{X}_k^{(l)}\|^2$ can be rewritten as

$$\begin{aligned}&\|\boldsymbol{A}_k^{(l)} - \boldsymbol{X}_k^{(l)}\|^2\\ =&\mathrm{tr}\left\{(\boldsymbol{A}_k^{(l)})^H\boldsymbol{A}_k^{(l)}\right\}+\mathrm{tr}\left\{(\boldsymbol{X}_k^{(l)})^H\boldsymbol{X}_k^{(l)}\right\}-2\mathrm{tr}\left\{(\boldsymbol{X}_k^{(l)})^H\boldsymbol{A}_k^{(l)}\right\}\\ =&\mathrm{tr}\left\{(\boldsymbol{A}_k^{(l)})^H\boldsymbol{C}_k^{(l)}\right\}+M-2\mathrm{tr}\left\{(\boldsymbol{X}_k^{(l)})^H\boldsymbol{A}_k^{(l)}\right\}. \end{aligned}\tag{23}$$

Thus, minimizing $\|\boldsymbol{A}_k^{(l)} - \boldsymbol{X}_k^{(l)}\|^2$ is equal to maximizing $\mathrm{tr}\left\{(\boldsymbol{X}_k^{(l)})^H\boldsymbol{A}_k^{(l)}\right\}$. As the first column of $\boldsymbol{X}_k^{(l)}$ is given, $\mathrm{tr}\left\{(\boldsymbol{X}_k^{(l)})^H\boldsymbol{A}_k^{(l)}\right\}$ is equal to $\mathrm{tr}\left\{(\boldsymbol{X}_{k[:,2:M]}^{(l)})^H\boldsymbol{A}_{k[:,2:M]}^{(l)}\right\}$ and it can be further rewritten as $\mathrm{tr}\left\{(\boldsymbol{X}_{k[:,2:M]}^{(l)})^H\hat{\boldsymbol{A}}_k^{(l)}\right\}$ with $\hat{\boldsymbol{A}}_k^{(l)} = \boldsymbol{A}_{k[:,2:M]}^{(l)} - \boldsymbol{a}_{k,1}\boldsymbol{a}_{k,1}^H\boldsymbol{A}_{k[:,2:M]}^{(l)}$ since $(\boldsymbol{X}_k^{(l)})^H\boldsymbol{X}_k^{(l)} = \boldsymbol{I}$. Given that the SVD of $\hat{\boldsymbol{A}}_k^{(l)}$ is $\boldsymbol{U}_k^{A,(l)}\boldsymbol{\Sigma}_k^{A,(l)}(\boldsymbol{V}_k^{A,(l)})^H$, we have

$$\begin{aligned}&\mathrm{tr}\left\{(\boldsymbol{X}_{k[:,2:M]}^{(l)})^H\hat{\boldsymbol{A}}_k^{(l)}\right\}\\ =&\mathrm{tr}\left\{(\boldsymbol{X}_{k[:,2:M]}^{(l)})^H\boldsymbol{U}_k^{A,(l)}\boldsymbol{\Sigma}_k^{A,(l)}(\boldsymbol{V}_k^{A,(l)})^H\right\}\\ =&\mathrm{tr}\left\{\boldsymbol{\Sigma}_k^{A,(l)}(\boldsymbol{V}_k^{A,(l)})^H(\boldsymbol{X}_{k[:,2:M]}^{(l)})^H\boldsymbol{U}_k^{A,(l)}\right\}. \end{aligned}\tag{24}$$

Since $\boldsymbol{\Sigma}_k^{A,(l)}$ is a diagonal matrix with the diagonal elements no less than zero, $(\boldsymbol{V}_k^{A,(l)})^H(\boldsymbol{X}_{k[:,2:M]}^{(l)})^H\boldsymbol{U}_k^{A,(l)}$ should be an identity matrix to maximize $\mathrm{tr}\left\{(\boldsymbol{X}_{k[:,2:M]}^{(l)})^H\hat{\boldsymbol{A}}_k^{(l)}\right\}$. Thus, $\boldsymbol{C}_k^{(l),\star} = \boldsymbol{U}_k^{A,(l)}(\boldsymbol{V}_k^{A,(l)})^H$, which ends the proof.

APPENDIX C
PROOF OF LEMMA 2

Assuming that the first column of $\boldsymbol{C}_k$ can be represented as a linear combination of the columns of $\boldsymbol{V}_k$ with the coefficient vector being $\boldsymbol{a}_{k,1}$, which can be expressed as

$$\begin{bmatrix}\boldsymbol{C}_{k[1:M,1]}\\ \boldsymbol{C}_{k[M+1:N,1]}\end{bmatrix} = \begin{bmatrix}\boldsymbol{V}_{k[1:M,:]}\\ \boldsymbol{V}_{k[M+1:N,:]}\end{bmatrix}\boldsymbol{a}_{k,1}. \tag{25}$$

It is noted that the rank of $\boldsymbol{V}_k$ is M, so $\boldsymbol{V}_{k[1:M,:]}$ is invertible. Thus, we have

$$\boldsymbol{a}_{k,1} = (\boldsymbol{V}_{k[1:M,:]})^{-1}\boldsymbol{C}_{k[1:M,1]}. \tag{26}$$

Then, $\boldsymbol{C}_{k[M+1:N,1]}$ can be calculated as

$$\boldsymbol{C}_{k[M+1:N,1]} = \boldsymbol{V}_{k[M+1:N,:]}(\boldsymbol{V}_{k[1:M,:]})^{-1}\boldsymbol{C}_{k[1:M,1]}, \tag{27}$$

which ends the proof.

REFERENCES

[1] Y. Wang, J. Liu, Y. Chen, M. Gruteser, J. Yang, and H. Liu, "E-eyes: Device-free location-oriented activity identification using fine-grained WiFi signatures," in *Proc. 20th ACM Annu. Int. Conf. Mobile Comput. Netw. (MobiCom)*, Sep. 2014, pp. 617–628.

[2] Y. Ren, S. Tan, L. Zhang, Z. Wang, Z. Wang, and J. Yang, "Liquid level sensing using commodity WiFi in a smart home environment," *Proc. ACM Interact. Mobile Wearable Ubiquitous Technol.*, vol. 4, no. 1, pp. 1–30, Mar. 2020.

[3] Y. Himeur, B. Rimal, A. Tiwary, and A. Amira, "Using artificial intelligence and data fusion for environmental monitoring: A review and future perspectives," *Inf. Fusion*, vol. 86, pp. 44–75, 2022.

[4] P. Asha, L. Natrayan, B. Geetha, J. R. Beulah, R. Sumathy, G. Varalakshmi, and S. Neelakandan, "IoT enabled environmental toxicology for air pollution monitoring using AI techniques," *Environ. Res.*, vol. 205, p. 112574, Apr. 2022.

[5] S. Tan, L. Zhang, and J. Yang, "Sensing fruit ripeness using wireless signals," in *Proc. 27th IEEE Int. Conf. Comput. Commun. Netw. (ICCCN)*, Jul. 2018, pp. 1–9.

[6] J. Liu, Y. Wang, Y. Chen, J. Yang, X. Chen, and J. Cheng, "Tracking vital signs during sleep leveraging off-the-shelf WiFi," in *Proc. 16th ACM Int. Symp. Mobile Ad Hoc Netw. Comput. (MobiHoc)*, Jun. 2015, pp. 267–276.

[7] V. Tarokh, N. Seshadri, and A. R. Calderbank, "Space-time codes for high data rate wireless communication: Performance criterion and code construction," *IEEE Trans. Inf. Theory*, vol. 44, no. 2, pp. 744–765, Mar. 1998.

[8] F. Liu, Y. Cui, C. Masouros, J. Xu, T. X. Han, Y. C. Eldar, and S. Buzzi, "Integrated sensing and communications: Toward dual-functional wireless networks for 6G and beyond," *IEEE J. Sel. Areas Commun.*, vol. 40, no. 6, pp. 1728–1767, Jun. 2022.

[9] T. Wild, V. Braun, and H. Viswanathan, "Joint design of communication and sensing for beyond 5G and 6G systems," *IEEE Access*, vol. 9, pp. 30 845–30 857, 2021.

[10] C. Dou, N. Huang, Y. Wu, L. Qian, and T. Q. Quek, "Sensing-efficient NOMA-aided integrated sensing and communication: A joint sensing scheduling and beamforming optimization," *IEEE Trans. Veh. Technol.*, vol. 72, no. 10, pp. 13 591–13 603, Oct. 2023.

[11] Y. He, Y. Cai, H. Mao, and G. Yu, "RIS-assisted communication radar coexistence: Joint beamforming design and analysis," *IEEE J. Sel. Areas Commun.*, vol. 40, no. 7, pp. 2131–2145, Jul. 2022.

[12] Y. He, J. Liu, M. Li, G. Yu, J. Han, and K. Ren, "*SenCom*: Integrated sensing and communication with practical WiFi," in *Proc. Annu. Int. Conf. Mob. Comput. Netw. (MobiCom)*, Oct. 2023, pp. 1–16.

[13] R. Lin, M. Soltanalian, B. Tang, and J. Li, "Efficient design of binary sequences with low autocorrelation sidelobes," *IEEE Trans. Signal Process.*, vol. 67, no. 24, pp. 6397–6410, Dec. 2019.

[14] S. Yang, D. Zhang, R. Song, P. Yin, and Y. Chen, "Multiple WiFi access points co-localization through joint AoA estimation," *IEEE Trans. Mobile Comput.*, vol. 23, no. 2, pp. 1488–1502, Feb. 2024.

[15] R. Yang, X. Yang, J. Wang, M. Zhou, Z. Tian, and L. Li, "Decimeter level indoor localization using WiFi channel state information," *IEEE Sensors J.*, vol. 22, no. 6, pp. 4940–4950, Mar. 2022.

[16] M. Kotaru, K. Joshi, D. Bharadia, and S. Katti, "Spotfi: Decimeter level localization using WiFi," in *Proc. ACM Conf. Special Interest Group Data Commun. (SIGCOMM)*, Aug. 2015, pp. 269–282.

[17] K. Qian, C. Wu, Z. Zhou, Y. Zheng, Z. Yang, and Y. Liu, "Inferring motion direction using commodity Wi-Fi for interactive exergames," in *Proc. ACM CHI*, May 2017, pp. 1961–1972.

[18] W. Jiang, C. Miao, F. Ma, S. Yao, Y. Wang, Y. Yuan, H. Xue, C. Song, X. Ma, D. Koutsonikolas, W. Xu, and L. Su, "Towards environment independent device free human activity recognition," in *Proc. 24th ACM Annu. Int. Conf. Mobile Comput. Netw. (MobiCom)*, Oct. 2018, pp. 289–304.

[19] "IEEE draft standard for information technology–telecommunications and information exchange between systems local and metropolitan area networks–specific requirements Part 11: Wireless LAN medium access control (MAC) and physical layer (PHY) specifications," *IEEE P802.11-REVmc*, pp. 1–3237, Nov. 2013.

[20] M. Silva, L. Ramalho, I. Almeida, E. Medeiros, and A. Klautau, "CSI compression for distributed-MIMO with centralized precoding and power allocation," *IEEE Commun. Lett.*, vol. 27, no. 6, pp. 1535–1539, Jun. 2023.

[21] F. Meneghello, C. Chen, C. Cordeiro, and F. Restuccia, "Toward integrated sensing and communications in IEEE 802.11 bf Wi-Fi networks," *IEEE Commun. Mag.*, vol. 61, no. 7, pp. 128–133, Jul. 2023.

[22] S. Tan and J. Yang, "WiFinger: Leveraging commodity WiFi for fine-grained finger gesture recognition," in *Proc. 17th ACM Int. Symp. Mobile Ad Hoc Netw. Comput. (MobiHoc)*, Jul. 2016, pp. 201–210.

[23] X. Wang, C. Yang, and S. Mao, "TensorBeat: tensor decomposition for monitoring multiperson breathing beats with commodity WiFi," *ACM Trans. Intell. Syst. Technol.*, vol. 9, no. 8, pp. 1–27, Sep. 2017.

[24] J. Wang, H. Jiang, J. Xiong, K. Jamieson, X. Chen, D. Fang, and B. Xie, "LiFS: Low human-effort, device-free localization with fine-grained subcarrier information," in *Proc. 22nd Annu. Int. Conf. Mobile Comput. Netw. (MobiHoc)*, Oct. 2016, pp. 243–256.

[25] Z. Jiang, T. H. Luan, X. Ren, D. Lv, H. Hao, J. Wang, K. Zhao, W. Xi, Y. Xu, and R. Li, "Eliminating the barriers: Demystifying Wi-Fi

baseband design and introducing the picoscenes Wi-Fi sensing platform," *IEEE Internet Things J.*, vol. 9, no. 6, pp. 4476–4496, 2021.
[26] F. Meneghello, F. Restuccia, and M. Rossi, "WHACK: Adversarial beamforming in MU-MIMO through compressed feedback poisoning," *IEEE Trans. Wireless Commun.*, 2024, early access, doi: 10.1109/TWC.2024.3452438.
[27] X. Li, J. Hu, and J. Luo, "Efficient beamforming feedback information-based WiFi sensing by feature selection," *IEEE Wireless Commun. Lett.*, vol. 13, no. 9, pp. 2347–2351, Sep. 2024.
[28] C. Wu, X. Huang, J. Huang, and G. Xing, "Enabling ubiquitous wifi sensing with beamforming reports," in *Proc. ACM Conf. Special Interest Group Data Commun. (SIGCOMM)*, Sep. 2023, pp. 20–32.
[29] J. Hu, T. Zheng, Z. Chen, H. Wang, and J. Luo, "MUSE-Fi: Contactless muti-person sensing exploiting near-field WiFi channel variation," in *Proc. 29th ACM Annu. Int. Conf. Mobile Comput. Netw. (MobiCom)*, Oct. 2023, pp. 1–15.
[30] Y. Jiang, Y. Gong, Y. Zeng, Y. Lv, T. X. Han, R. Ding, and R. Du, "On the design and performance of QRD-based beamforming feedback for Wi-Fi sensing," *IEEE Trans. Wireless Commun.*, vol. 23, no. 5, pp. 5261–5271, May 2024.
[31] C. Li, M. Liu, and Z. Cao, "WiHF: Gesture and user recognition with WiFi," *IEEE Trans. Mobile Comput.*, vol. 21, no. 2, pp. 757–768, Feb. 2022.
[32] R. H. Venkatnarayan, S. Mahmood, and M. Shahzad, "WiFi based multi-user gesture recognition," *IEEE Trans. Mobile Comput.*, vol. 20, no. 3, pp. 1242–1256, Mar. 2021.
[33] R. Burkholder, L. Gupta, and J. Johnson, "Comparison of monostatic and bistatic radar images," *IEEE Antennas Propag. Mag.*, vol. 45, no. 3, pp. 41–50, Jun. 2003.
[34] O. Renaudin, T. Zemen, and T. Burgess, "Ray-tracing based fingerprinting for indoor localization," in *Proc. IEEE Work. Signal Process. Adv. Wireless Commun. (SPAWC)*, Jun. 2018, pp. 1–5.
[35] X. Zhang, Y. Zhang, G. Liu, and T. Jiang, "AutoLoc: Toward ubiquitous AoA-based indoor localization using commodity WiFi," *IEEE Trans. Veh. Technol.*, vol. 72, no. 6, pp. 8049–8060, Jun. 2023.
[36] J. Xiong and K. Jamieson, "ArrayTrack: A fine-grained indoor location system," in *Proc. 10th USENIX Symp. Netw. Syst. Design Implement. (NSDI)*, Apr. 2013, pp. 71–84.
[37] Y. Ren, Z. Wang, Y. Wang, S. Tan, Y. Chen, and J. Yang, "GoPose: 3D human pose estimation using WiFi," *Proc. ACM Interact. Mo.*, vol. 6, no. 2, pp. 1–25, Jul. 2022.
[38] Y. Wang, Y. Ren, Y. Chen, and J. Yang, "Wi-mesh: A WiFi vision-based approach for 3D human mesh construction," in *Pro. 20th ACM Conf. Embedded Netw. Sen. Sys. (SenSys)*, Jan. 2023, pp. 362–376.
[39] C. Ma, B. Wu, S. Poslad, and D. R. Selviah, "Wi-Fi RTT ranging performance characterization and positioning system design," *IEEE Trans. Mobile Comput.*, vol. 21, no. 2, pp. 740–756, Feb. 2022.
[40] J. Xiong, K. Sundaresan, and K. Jamieson, "ToneTrack: Leveraging frequency-agile radios for time-based indoor wireless localization," in *Proc. 21st ACM Annu. Int. Conf. Mobile Comput. Netw. (MobiCom)*, Sep. 2015, pp. 537–549.
[41] H. Xue, J. Yu, F. Lyu, and M. Li, "Push the limit of multipath profiling using commodity WiFi devices with limited bandwidth," *IEEE Trans. Veh. Technol.*, vol. 69, no. 4, pp. 4142–4154, Apr. 2020.
[42] Z. Li, Z. Tian, and M. Zhou, "Decimeter level indoor localization using hybrid measurements of a distributed single receiver," *IEEE Trans. Instrum. Meas.*, vol. 70, pp. 1–14, 2021.
[43] W. Wang, A. X. Liu, M. Shahzad, K. Ling, and S. Lu, "Understanding and modeling of WiFi signal based human activity recognition," in *Proc. 21st ACM Annu. Int. Conf. Mobile Comput.Netw. (MobiCom)*, Sep. 2015, pp. 65–76.
[44] Y. He, J. Liu, M. Li, G. Yu, and J. Han, "Forward-compatible integrated sensing and communication for WiFi," *IEEE J. Sel. Areas Commun.*, vol. 42, no. 9, pp. 2440–2456, Sep. 2024.
[45] J. Liu, Y. Wang, Y. Chen, J. Yang, X. Chen, and J. Cheng, "Tracking vital signs during sleep leveraging off-the-shelf WiFi," in *Proc 16th ACM Int. Symp. Mobile Ad Hoc Netw. Comput. (MobiHoc)*, Jun. 2015, pp. 267–276.
[46] G. Wang, Y. Zou, Z. Zhou, K. Wu, and L. M. Ni, "We can hear you with WiFi!" in *Proc. 20th ACM Annu. Int. Conf. Mobile Comput. Netw. (MobiCom)*, Sep. 2014, pp. 593–604.
[47] V. Klema and A. Laub, "The singular value decomposition: Its computation and some applications," *IEEE Trans. Autom. Control*, vol. 25, no. 2, pp. 164–176, Apr. 1980.
[48] E. Perahia and R. Stacey, *Next Generation Wireless LANs: 802.11 n and 802.11 ac*. Cambridge University Press, 2013.
[49] X. Feng and C. Leung, "A new optimal transmit and receive diversity scheme," in *Proc. IEEE PACRIM*, vol. 2, Aug. 2001, pp. 538–541.
[50] P. A. Dighe, R. K. Mallik, and S. S. Jamuar, "Analysis of transmit-receive diversity in Rayleigh fading," *IEEE Trans. Commun.*, vol. 51, no. 4, pp. 694–703, Apr. 2003.
[51] O. Bejarano, E. W. Knightly, and M. Park, "IEEE 802.11ac: From channelization to multi-user MIMO," *IEEE Commun. Mag.*, vol. 51, no. 10, pp. 84–90, Oct. 2013.
[52] Y. Ding, T. N. Davidson, Z.-Q. Luo, and K. M. Wong, "Minimum BER block precoders for zero-forcing equalization," *IEEE Trans. Signal Process.*, vol. 51, no. 9, pp. 2410–2423, Sep. 2003.
[53] S.-T. Zhou, D. Wang, Q. Xiao, J.-m. Zhou, H.-G. Li, and W.-B. Tu, "An improved first order reliability method based on modified Armijo rule and interpolation-based backtracking scheme," *Proc. Inst. Mech. Eng. O*, vol. 235, no. 2, pp. 209–229, Sep. 2020.
[54] Å. Björck, "Numerics of gram-schmidt orthogonalization," *Linear Algebra Appl.*, vol. 197, pp. 297–316, Jan. 1994.
[55] J. K. Cullum and R. A. Willoughby, *Lanczos Algorithms for Large Symmetric Eigenvalue Computations: Vol. I: Theory*. SIAM, 2002.
[56] R. Schmidt, "Multiple emitter location and signal parameter estimation," *IEEE Trans. Antennas Propagat.*, vol. 34, no. 3, pp. 276–280, Mar. 1986.
[57] Y. He, G. Yu, Y. Cai, and H. Luo, "Integrated sensing, computation, and communication: System framework and performance optimization," *IEEE Trans. Wireless Commun.*, vol. 23, no. 2, pp. 1114–1128, Feb. 2024.
[58] S. W. Drury, "A generalization of von Neumann's inequality to the complex ball," *Proc. Amer. Math. Soc.*, vol. 68, no. 3, pp. 300–304, Dec. 1978.

Lei Huang received the B.E. degree in electronics and information engineering from Hangzhou Dianzi University, Hangzhou, China, in 2023. He is pursuing the M.E. degree with the College of Information Science and Electronic Engineering, Zhejiang University, Hangzhou, China. His research interests mainly include waveform design and CSI compression in integrated sensing and communication (ISAC).

Yinghui He (Member, IEEE) received the B.E. degree in information engineering and Ph.D. degree in information and communication engineering from Zhejiang University, Hangzhou, China, in 2018 and 2023, respectively. His research interests mainly include integrated sensing and communications (ISAC), mobile computing, and device-to-device communications.

Guanding Yu (Senior Member, IEEE) received the B.E. and Ph.D. degrees in communication engineering from Zhejiang University, Hangzhou, China, in 2001 and 2006, respectively. He joined Zhejiang University in 2006, and is now a Professor with the College of Information and Electronic Engineering. From 2013 to 2015, he was also a Visiting Professor at the School of Electrical and Computer Engineering, Georgia Institute of Technology, Atlanta, GA, USA. His research interests include integrated sensing and communications (ISAC), mobile edge computing/learning, and machine learning for wireless networks.

Dr. Yu has served as a guest editor of IEEE Communications Magazine special issue on Full-Duplex Communications, an Editor of IEEE Journal on Selected Areas in Communications Series on Green Communications and Networking, and Series on Machine Learning in Communications and Networks, an Editor of IEEE Wireless Communications Letters, a lead Guest Editor of IEEE Wireless Communications Magazine special issue on LTE in Unlicensed Spectrum, an Editor of IEEE Transactions on Green Communications and Networking, and an Editor of IEEE Access. He is now serving as an editor of *IEEE Transactions on Machine Learning in Communications and Networking*. He received the 2016 IEEE ComSoc Asia-Pacific Outstanding Young Researcher Award. He regularly sits on the technical program committee (TPC) boards of prominent IEEE conferences such as ICC, GLOBECOM, and VTC. He also serves as a Symposium Co-Chair for IEEE GLOBECOM 2019 and a Track Chair for IEEE VTC 2019'Fall.

Jianfeng Wang received the B.E. and Ph.D degrees in Communication Engineering from Beijing University of Posts and Telecommunications, Beijing, China, in 2003 and 2008, respectively. In 2008, he joined Ericsson Research, working on 3GPP standardization on LTE and NR, and joined Intel Lab in 2017 working on AI/ML for wireless research. Since 2021, he has been a Senior Researcher for wireless research in Lenovo Research. His research interests include MIMO, AI/ML, and ISAC.

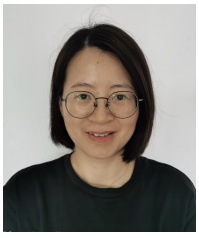

Haiyan Luo received the B.E. and Ph.D. degrees in communication engineering from Zhejiang University, Hangzhou, China, in 2005 and 2010, respectively. She joinded Huawei Technology Co., Ltd in 2010 mainly working on 3GPP standard research. From 2021, she joined Lenovo as a senior researcher for wireless research. Her research interests include 5GC architecture enhancement, AIML, XR, and sensing.